Resolving Complexity in the Interactions of Redox Enzymes and Their Inhibitors: Contrasting Mechanisms for the Inhibition of a Cytochrome *c* Nitrite Reductase Revealed by Protein Film Voltammetry†

James D. Gwyer,‡ David J. Richardson,§ and Julea N. Butt*,‡,§

Centre for Metalloprotein Spectroscopy and Biology, School of Chemical Sciences and Pharmacy and School of Biological Sciences, University of East Anglia, Norwich NR4 7TJ, U.K.

Received May 6, 2004; Revised Manuscript Received September 18, 2004

ABSTRACT: Cytochrome *c* nitrite reductase is a dimeric decaheme-containing enzyme that catalyzes the reduction of nitrite to ammonium. The contrasting effects of two inhibitors on the activity of this enzyme have been revealed, and defined, by protein film voltammetry (PFV). Azide inhibition is rapid and reversible. Variation of the catalytic current magnitude describes mixed inhibition in which azide binds to the Michaelis complex ($K_d^M \sim 40$ mM) with a lower affinity than to the enzyme alone ($K_d^E \sim 15$ mM) and leads to complete inhibition of enzyme activity. The position of the catalytic wave reports tighter binding of azide when the active site is oxidized ($K_d^O \sim 39$ μM) than when it is reduced. By contrast, binding and release of cyanide are sluggish. The higher affinity of cyanide for reduced versus oxidized forms of nitrite reductase is immediately revealed, as is the presence of two sites for cyanide binding and inhibition of the enzyme. Formation of the monocyano complex by reduction of the enzyme followed by a "rapid" scan to high potentials captures the activity−potential profile of this enzyme form and shows it to be distinct from that of the uninhibited enzyme. The biscyano complex is inactive. These studies demonstrate the complexity that can be associated with inhibitor binding to redox enzymes and illustrate how PFV readily captures and deconvolves this complexity through its impact on the catalytic properties of the enzyme.

Redox enzymes are characterized by their ability to couple long-range electron transfer with catalysis. Within such enzymes, at least one center couples a change of oxidation state to events such as bond breakage and formation, ligand binding, or conformational change to define the pathway by which substrates are transformed to products. This intimate relationship between redox-linked chemistries and progress through the catalytic cycle provides a considerable opportunity for electrochemical potential to modulate redox enzyme activity. In a first approximation, the reduction potentials of centers within the enzyme define potentials at which modulations of activity can be anticipated. In practice, the operational reduction potentials can show marked deviations from those measured at equilibrium; they may be modulated by association of the substrate with the enzyme or when the electron flux achieved during catalysis is sufficient to tune out slower, redox-linked chemical or conformational events (*1*, *2*). The result is a dependence of the catalytic rate on electrochemical potential that informs on the mechanisms and regulation of redox enzyme activity.

Protein film voltammetry (PFV)[1] provides a ready resolution of enzyme activity across the electrochemical potential domain (*3*). The enzyme of interest is adsorbed on an electrode surface in such a way that there is direct and facile electron exchange between them. Changes in oxidation state induced by the electrode potential are reversed by the transformation of the substrate to product during catalysis, and enzyme turnover is quantitated by the corresponding flow of "catalytic" current. Activity (current)−potential profiles defined by cyclic voltammetry reveal boosts and attenuations of activity due to modulation of the rates of processes intrinsic to the catalytic mechanism (*4*−*15*). These modulations are characteristic of each enzyme and the turnover conditions, e.g., substrate concentration and pH, employed. They have been variously attributed to redox-linked chemistries associated with active site centers or the consequence of oxidation-state change at centers remote from the active site and normally considered electron relay stations. In each case, they have provided fresh mechanistic insights into the enzymes under investigation.

We recently employed PFV to complement structural and more conventional time-resolved studies of *Escherichia coli* cytochrome *c* nitrite reductase (*15*, *16*). This enzyme catalyzes the six-electron reduction of nitrite to ammonium ($K_M \sim 26$ μM) within a homodimeric structure containing 10 *c*-type hemes (Figure 1A). Activation of nitrite reductase activity is detected as a negative (reductive) current that

† This work was funded by the EPSRC (DTA award to J.D.G.), the BBSRC through Grants 83/B17233, 6/P11528, and 83/B18695, and funding of the Centre for Metalloprotein Spectroscopy and Biology at University of East Anglia in addition to JIF Award 062178.

* To whom correspondence should be addressed. Telephone: 44 1603 593877. Fax: 44 1603 592003. E-mail: j.butt@uea.ac.uk.

‡ School of Chemical Sciences and Pharmacy.

§ School of Biological Sciences.

[1] Abbreviations: HAO, *Nitrosomonas europaea* hydroxylamine oxidoreductase; NrfA, *Escherichia coli* cytochrome *c* nitrite reductase; PFV, protein film voltammetry; PGE, pyrolytic graphite "edge"; RDE, rotating disc electrode; SHE, standard hydrogen electrode.

10.1021/bi049085x CCC: $27.50
Published on Web 11/05/2004

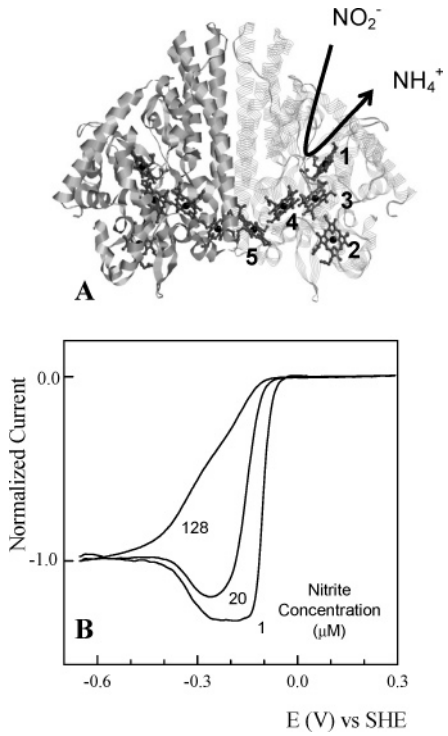

FIGURE 1: *E. coli* cytochrome *c* nitrite reductase. (A) Structure of the enzyme with the hemes of one monomer numbered according to the order in which their CxxC binding motifs occur in the amino acid sequence. (B) Steady-state catalytic waveforms displayed by films of cytochrome *c* nitrite reductase in 1, 20, and 128 μM nitrite at pH 7, with a scan rate of 30 mV s^{-1} and electrode rotation rate of 3000 rpm. The waveforms have been normalized to emphasize their different features; the final relative magnitudes of current at -0.6 V are 1, 11.6, and 21.7 for 1, 20, and 128 μM nitrite, respectively. The same information is portrayed as derivative plots (d*i*/d*E*) in Figure 3 of ref *15*.

requires the application of potentials well below the NO_2^-/NH_4^+ couple ($E_{m,7} = 340$ mV) (Figure 1B). A further increase in the driving force for the reaction being catalyzed leads to attenuation of the nitrite-limited turnover rate but boosts the rate of turnover under enzyme-limited conditions.

The nitrite-limited waveform is rationalized by correlation with reduction potentials defined by potentiometric titration of the enzyme monitored by electron paramagnetic resonance (EPR) spectroscopy (*15*, *16*). Activity is initiated by reduction of the heme 1,3 pair ($E_{m,7} = -103$ mV, $n = 2$). Heme 1 has axial ligands provided by a lysine side chain and water (hydroxide), with the latter ligand being displaced when nitrite binds to the enzyme (*17*). Heme 3 has bishistidine axial ligation, and its porphyrin ring lies parallel to that of heme 1, placing the porphyrin rings within 4.5 Å at the point of closest approach. The attenuation of activity at lower potentials correlates with the reduction of bishistidine-coordinated hemes 4 and 5 that lie near the dimer interface (for each center, $E_{m,7} \sim -323$ mV). It remains to be established whether this reduction has an adverse effect on a conformational or electronic contribution to catalysis. There is no evidence that the oxidation state of the bishistidine-coordinated heme 2 ($E_{m,7} \sim -37$ mV) has an effect on nitrite reductase activity.

At higher nitrite concentrations, the low-potential attenuation is "tuned out". The process that gives rise to it is too slow to engage under conditions of rapid substrate association with the enzyme. The boost of activity that emerges at lower potentials has a position dependent on substrate concentration and so is unlikely to arise from reduction of hemes 4 and 5. The waveform describing enzyme-limited turnover may reflect rate definition by gated-electron delivery to the heme 1,3 pair (*4*, *8*).

Electrochemical potential, via the oxidation state, can also influence enzyme activity through modulation of the affinity for inhibitors (*12*, *18*). Cyanide and azide are known inhibitors of cytochrome *c* nitrite reductase, but little information about their mechanism(s) of inhibition is available (*19*, *20*). Here we use PFV to visualize and define the contrasting mechanisms employed by these inhibitors and at the same time shed greater light on the operation of a key N-cycle enzyme.

EXPERIMENTAL PROCEDURES

Cytochrome *c* nitrite reductase (NrfA) was purified from *E. coli* as described previously and stored as aliquots in liquid nitrogen (*16*). Samples had a specific activity of 1500 μmol of nitrite consumed min^{-1} mg^{-1} ($k_{cat} = 7930$ electrons s^{-1} $monomer^{-1}$) in 50 mM Hepes and 2 mM $CaCl_2$ (pH 7.0) using dithionite-reduced methyl viologen as the electron donor. Concentrations of the air-equilibrated enzyme ($A_{410}/A_{280} = 2.5$) were determined using an ϵ_{410} of 497 650 M^{-1} cm^{-1} (*16*).

All chemicals were of Analar quality or better. Solutions were prepared in water with a resistivity of >18 MΩ cm (Purelab Maxima, ELGA). A buffer/electrolyte solution composed of 50 mM Hepes and 2 mM $CaCl_2$ (pH 7.0) was used for all experiments and the preparation of stock solutions unless stated otherwise. A fresh $NaNO_2$ stock solution was prepared each day by dissolution of the appropriate mass in the ice-cold buffer/electrolyte solution. Solutions of the desired azide concentration were prepared by dilution of a 5 M NaN_3 stock solution. A KCN stock solution was prepared by dissolution in water and the cyanide concentration determined to be 490 mM by titration against silver nitrate (*21*). The stock solution was diluted in the buffer/electrolyte solution to provide cyanide solutions of the desired concentration. Measurement of the solution pH before experimentation and after removal from the electrochemical cell confirmed that the pH was 7.0. Replacement of $NaNO_2$ with KNO_2 produced no detectable change in the results.

Voltammetry was performed using a three-electrode cell configuration with the sample chamber thermostated at 25 °C (*11*). The Ag/AgCl reference electrode was used (saturated KCl), and the counter electrode a platinum wire. The cell was housed in a Faraday cage inside a nitrogen-filled anaerobic chamber (atmospheric O_2 level of <5 ppm). Immediately prior to each experiment, the pyrolytic graphite edge (PGE) working electrode (3 mm diameter) was polished with an aqueous 0.3 μm alumina slurry, sonicated, rinsed, and dried with a tissue. An ice-cold 1 μL aliquot of 0.65 μM nitrite reductase in 2 mM $CaCl_2$ and 50 mM Hepes (pH 7.0) was placed on the electrode for ca. 10 s; excess solution was removed, and the electrode was immediately placed into the electrochemical cell. Electrode rotation was achieved with an EG&G model 306 rotator. Voltammetry and chronoamperometry were performed with an AutolabPGSTAT 30 instrument under the control of GPES software. All potentials

are reported relative to the standard hydrogen electrode (SHE) following addition of 0.197 V to the experimental potential.

Control experiments performed with freshly polished "bare" PGE electrodes in solutions composed of the nitrite, cyanide, or azide concentrations described in this work produced baselines with no evidence of Faradaic current. A small but reproducible increase in the charging current was noted when experiments were performed with the enzyme film in place. To compensate for this effect, the charging current of the appropriate baseline was scaled to match that of the voltammogram with the film in place prior to baseline subtraction. Values of E_{cat} were obtained from the position of the appropriate peak in a plot of the first derivative of the catalytic current versus applied potential.

For a given inhibitor concentration, the catalytic parameters K_M and V_{max} (i_{max}) were determined from a single film poised at −403 mV. Following each addition of nitrite, the electrode was rotated at various speeds to allow the current at infinite rotation rate (i_{cat}^{∞}) to be obtained through a Koutecky−Levich analysis (*15*). Where instability of the film necessitated, values of i_{cat}^{∞} were corrected for a first-order loss of signal intensity with time (i.e., for the uninhibited response, for all azide concentrations, and for cyanide concentrations of <1 μM). Comparison of the response from each film under standard conditions (20 μM nitrite without inhibitor) was used to account for slight film-to-film variation in the signal magnitude. Hanes plots of the resulting data allowed values of K_M and V_{max} to be defined through a linear fit using Microcal Origin.

Spectrophotometric assays of nitrite reductase activity were performed anaerobically in cuvettes containing 1 mM methyl viologen and appropriate concentrations of nitrite and inhibitor in 3 mL of buffer/electrolyte solution. Dithionite was added to give a stable absorbance of 2 at 600 nm and the reaction initiated by the addition of 0.33 μg of enzyme. Rates of methyl viologen oxidation were calculated using an ϵ_{600} of 13 700 M^{-1} cm^{-1}, Hanes plots were constructed and analyzed as described above.

RESULTS

At 30 mV s^{-1} with an electrode rotation rate of 3000 rpm, PFV of cytochrome *c* nitrite reductase in 20 μM nitrite shows a peak of activity at −290 mV (Figure 2A). Under these conditions, the catalytic currents of the forward and reverse scans overlay, experience minimal limitation from substrate mass transport, and reflect steady-state turnover (*15*). Enzyme activity is diminished by the introduction of millimolar concentrations of sodium azide (Figure 2A) or micromolar concentrations of potassium cyanide (Figure 3), in agreement with the previously reported potencies of these inhibitors (*19*). Interestingly, the catalytic wave shapes are also changed by the presence of the inhibitors. Azide induces a displacement of the peak of activity toward more negative potentials (Figure 2A). Cyanide induces dramatic and distinct changes to the activity−potential profiles of the forward and reverse sweeps (Figure 3). However, both azide and cyanide inhibition are fully reversible. Returning the films to solutions of 20 μM nitrite restores the wave shape to that of the uninhibited enzyme, and the catalytic current magnitudes return to within 90% of those seen prior to exposure to the inhibitors.

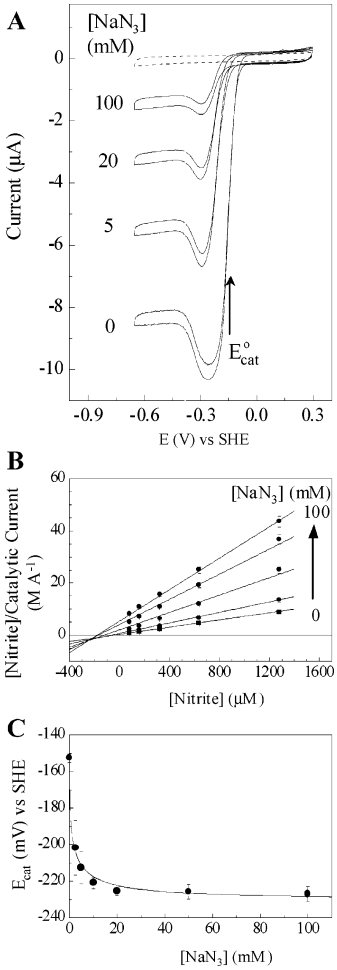

FIGURE 2: Azide inhibition of *E. coli* cytochrome *c* nitrite reductase. (A) Cyclic voltammograms from an enzyme film in 20 μM nitrite and the indicated azide concentrations (—). Voltammogram at a bare electrode in 20 μM nitrite (- - -). Other conditions: 50 mM Hepes, 2 mM $CaCl_2$, pH 7.0, 25 °C, scan rate of 30 mV s^{-1}, and electrode rotation rate of 3000 rpm. (B) Hanes plot for nitrite reduction by a film poised at −403 mV in 0, 10, 25, 50, and 100 mM azide. (C) Variation of E_{cat} with azide concentration for catalysis in 20 μM nitrite. (—) Best fit to eq 1 with the following: $K_d^O = 39$ μM, $K_d^R = 17.6$ mM, and $E_{cat}^0 = -152.5$ mV.

The simplest mechanism for reversible inhibition of cytochrome *c* nitrite reductase involves rapid, reversible binding of the inhibitor as the distal ligand to heme 1 with an affinity that is independent of enzyme oxidation state. In this scenario, inhibition is competitive and the catalytic wave at each inhibitor concentration is simply determined by the amount and catalytic properties of active, i.e., uninhibited, enzyme. As the concentration of such an inhibitor increases, the magnitude of the catalytic wave will decrease in direct proportion to the population of the active enzyme. The catalytic properties of the active enzyme are not changed by the presence of an inhibitor, so the shape and position of features within the catalytic wave are independent of inhibitor concentration.

Voltammetry with neither azide- nor cyanide-inhibited films of cytochrome *c* nitrite reductase conforms to the behavior described above. The implications for the mechanism of inhibition in each case are discussed separately below.

Azide Inhibition of Nitrite Reductase. Steady-state voltammograms are observed in the presence of azide, showing

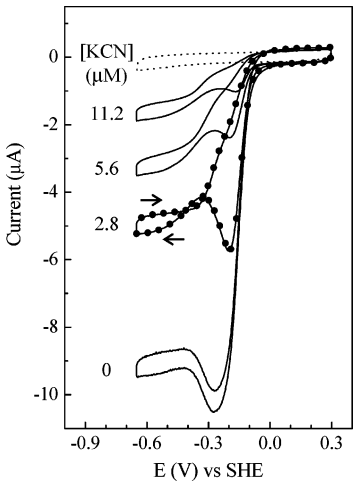

FIGURE 3: Cyclic voltammograms from a film of *E. coli* cytochrome *c* nitrite reductase in 20 μM nitrite and the indicated cyanide concentrations. Second cyclic voltammogram recorded after scanning was initiated at 0.3 V under the stated conditions (—). Third cyclic voltammogram in 2.8 μM cyanide (●), where arrows indicate the scan direction. Voltammogram recorded at a bare electrode in 20 μM nitrite (···). All other conditions were as described in the legend of Figure 2A.

that there is rapid equilibration of the inhibitor with the enzyme (Figure 2A). Catalytic current magnitudes quantitated at −403 mV for a range of azide and nitrite concentrations as described in Experimental Procedures are presented as a Hanes plot in Figure 2B. The decrease in apparent maximum velocity (V_{max}^{app}) and the increase in the apparent Michaelis constant (K_M^{app}) as the azide concentration is increased are typical of mixed inhibition where the affinity of the inhibitor for the Michaelis complex is weaker than for the enzyme. Following the Cornish−Bowden method, plots of K_M^{app}/V_{max}^{app} and $1/V_{max}^{app}$ against azide concentration were found to be linear, yielding a K_d^E of 11 ± 8 mM and a K_d^M of 39 ± 8 mM as the dissociation constants for azide binding to the enzyme and Michaelis complex, respectively (*22*).

In addition to the inhibition of activity induced by the presence of azide, it is apparent that lower potentials must be applied to "turn on" nitrite reductase activity by reduction of the heme 1,3 pair (Figure 2A). Quantitation of this feature shows that its steepness is insensitive to changes in azide concentration despite displacement of the potential (E_{cat}) at its steepest point (Figure 2C). Thus, azide has a higher affinity for the enzyme when the heme 1,3 pair is oxidized than when the heme 1,3 pair is reduced but does not alter the cooperativity of electron transfer at these centers.

Reversible binding of azide to nitrite reductase can be described by a four-species square scheme based around the reversible two-electron reduction of the heme 1,3 pair (Figure 4). Correlating E_{cat} with the apparent reduction potential of the heme 1,3 pair gives

$$E_{cat} = E_{cat}^0 + \frac{RT}{nF}\ln\left(\frac{1 + [N_3^-]/K_d^R}{1 + [N_3^-]/K_d^O}\right) \quad (1)$$

where E_{cat}^0 is the operating potential of the enzyme in the absence of azide, $[N_3^-]$ is the azide concentration, and K_d^O and K_d^R are the dissociation constants for azide binding to the enzyme with the heme 1,3 pair oxidized and reduced,

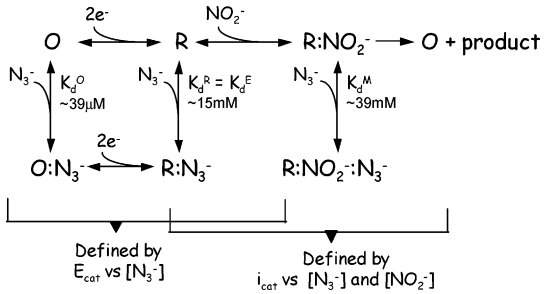

FIGURE 4: Thermodynamic description of azide binding to *E. coli* cytochrome *c* nitrite reductase derived from protein film voltammetry. O and R represent the enzyme with the heme 1,3 pair oxidized and reduced, respectively.

respectively. The electron stoichiometry (*n*) equals 2, and *R*, *T*, and *F* have their usual meanings. Variation of E_{cat} with azide concentration in 20 μM nitrite is described well by eq 1 with a K_d^O of 39 ± 10 μM and a K_d^R of 17 ± 5 mM (Figure 2C). Similar dissociation constants were obtained from experiments performed with lower nitrite concentrations supporting the assumptions implicit in the use of eq 1 in the present context, namely, that E_{cat} experiences a negligible influence of the feature describing the attenuation of activity at lower potentials and reflects the reduction potential of the heme 1,3 pair at the nitrite concentrations used in these experiments.

The similarity between K_d^R and K_d^E, derived from variation of E_{cat} and i_{cat}, respectively with azide concentration, indicates their reflection of the same equilibrium. The resulting thermodynamic description of the azide inhibition of cytochrome *c* nitrite reductase is illustrated in Figure 4. Since product is only generated from enzyme to which azide is not bound, the persistence of the attenuation of activity at lower potentials in the presence of azide is explained. The "foot" of the attenuation is independent of azide concentration as indicated by the vertical line in Figure 2A because it reflects the reduction potential of hemes 4 and 5 in the uninhibited enzyme. The width of the attenuation feature decreases as the azide concentration is increased since it is increasingly eclipsed by the displacement of the feature that describes the onset of activity.

Cyanide Inhibition of Nitrite Reductase. Voltammetry at 30 mV s^{-1} in the presence of cyanide produces inequivalent current−potential profiles for the forward and reverse sweeps, toward more negative and more positive potentials, respectively (Figure 3). Most significantly, a peak of activity on the forward sweep is absent from the return.

Comparison of the voltammetry in 0 and 2.8 μM cyanide suggests the explanation. These voltammograms, recorded with the same enzyme film, exhibit similar catalytic currents as catalysis is initiated on the forward scan. Only when the potential drops below ca. −200 mV does inhibition of activity in the cyanide solution become apparent. Activity then remains at an inhibited level until all detectable signs of catalysis are lost upon returning to most positive potentials on the reverse sweep. Allowing cyclic voltammetry to continue in the cyanide-containing solution produces exactly the same activity−potential profile (Figure 3, symbols). The film *regains* its activity at positive potentials, and inhibition is triggered once again by exposure to lower potentials. Cyanide has a lower affinity for oxidized than for more

reduced states of cytochrome *c* nitrite reductase. At higher cyanide concentrations, the extent of inhibition is greater and so is the rate of inhibition, the peak describing cyanide binding to the enzyme becoming smaller and displaced toward more positive potentials.

None of the voltammograms recorded in the presence of cyanide provide evidence for an increase in activity upon sweeping toward more positive potentials that would indicate release of cyanide during this part of the voltammogram. The activity−potential profiles of the reverse sweeps must reflect catalysis from *cyanide-bound enzyme*. This profile is distinct from that of the uninhibited enzyme; most notably, the attenuation of activity at low potential is absent, and so the rate-defining events of catalysis in these two forms of the enzyme must also be distinct. That addition of sufficiently high cyanide concentrations (ca. 70 μM) leads to the complete loss of the catalytic response (not shown) indicates the presence of a second, lower-affinity site for cyanide association with the enzyme that when fully occupied results in complete inhibition of activity.

Confirmation and further elucidation of the two modes for cyanide binding to, and inhibition of, nitrite reductase are provided by a steady-state analysis. Lowering the scan rate to 1 mV s^{-1} produces essentially superimposable activity−potential profiles for the forward and reverse sweeps, showing that steady-state turnover can be achieved in a reasonable time frame (Figure 5). Hanes plots derived from films poised at −403 mV, i.e., in experiments with an infinitely slow scan rate, are illustrated in Figure 6A. Introduction of up to 2 μM cyanide results in noncompetitive inhibition; at ca. 30 μM, V_{max}^{app} decreases but K_M^{app} remains constant. A further increase in the cyanide concentration continues to diminish V_{max}^{app}, but this is now accompanied by an increase in K_M^{app} to ca. 150 μM. The low catalytic currents introduce some uncertainty into the analysis at the higher cyanide concentrations but suggests noncompetitive inhibition may also accompany binding of the second cyanide molecule.

A simple mechanism that combines the steady-state and dynamic descriptions of nitrite reductase inhibition by cyanide is presented in Figure 6B. Cyanide binds with higher affinity to a reduced form of the enzyme, R, than to its oxidized state; given the potential window in which this process occurs, it is likely that it is triggered by reduction of the heme 1,3 pair. The monocyano complex retains nitrite reductase activity, and its affinity for cyanide is not altered by formation of the Michaelis complex. Inspection of the reverse sweeps from voltammetry at 30 mV s^{-1} during titration of cyanide into solutions with a fixed nitrite concentration indicates that the dissociation constant for binding of the first cyanide molecule to the reduced enzyme ($K_d^{E1} = K_d^{M1}$) is on the order of ~0.5 μM (see the Supporting Information). Occupation of the second cyanide-binding site leads to formation of a biscyano complex that lacks nitrite reductase activity. Inhibition of the monocyano complex in this way is suggested to be noncompetitive ($K_d^{E2} = K_d^{M2} \sim 8$ μM).

The monocyano complex predominates when the enzyme is reduced in the presence of 2−4 μM cyanide. This can be used together with the variable time scale accessible to PFV to define the activity−potential profile of the monocyano

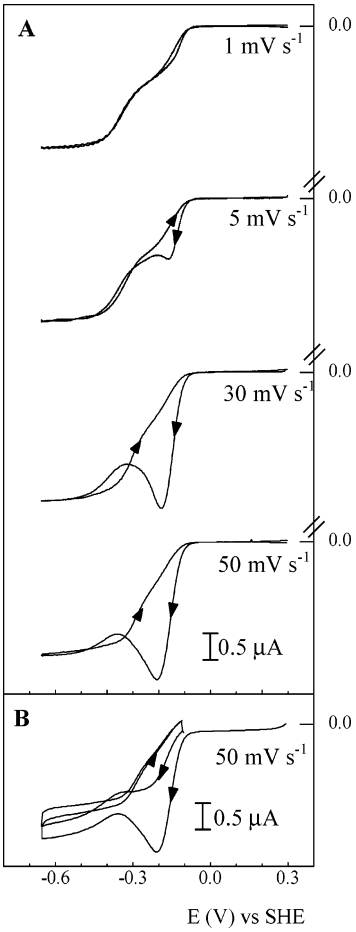

FIGURE 5: Scan rate dependence of the cyclic voltammetry with a film of *E. coli* cytochrome *c* nitrite reductase in 20 μM nitrite and 4 μM KCN. (A) Baseline-subtracted voltammograms, scan rates, and sweep directions as indicated. (B) Voltammetry carried out at 50 mV s^{-1} with a second scan initiated by reversing the sweep direction at −100 mV. Other experimental conditions were as described in the legend of Figure 2A.

adduct under conditions where it is most informatively compared to that of the uninhibited enzyme. Voltammetry at scan rates from 1 to 50 mV s^{-1} produces the same catalytic current at −600 mV, reporting full equilibration of cyanide with the enzyme by this point in each scan (Figure 5A). Changing the scan direction at −150 mV on the reverse sweep confirms that the monocyano complex persists throughout the reverse sweeps of voltammetry at 30 and 50 mV s^{-1} (see, for example, Figure 5B).

A comparison between the activity−potential profiles during nitrite-limited turnover of the monocyano complex and the uninhibited enzyme is depicted in Figure 7. Under these conditions, the features within the activity−potential profile of the uninhibited enzyme are well separated and correlate with the reduction potentials of specific heme centers (*15*). Activity from the uninhibited enzyme is turned on by cooperative two-electron reduction of the heme 1,3 pair, while the corresponding feature in the wave from the monocyano complex is centered on −127 mV and has the width expected for a one-electron process. Thus, the lower turnover number of the monocyano complex appears to be a consequence of an uncoupling of the electron transfer cooperativity between hemes 1 and 3. The boost of activity displayed on further reduction of the monocyano complex

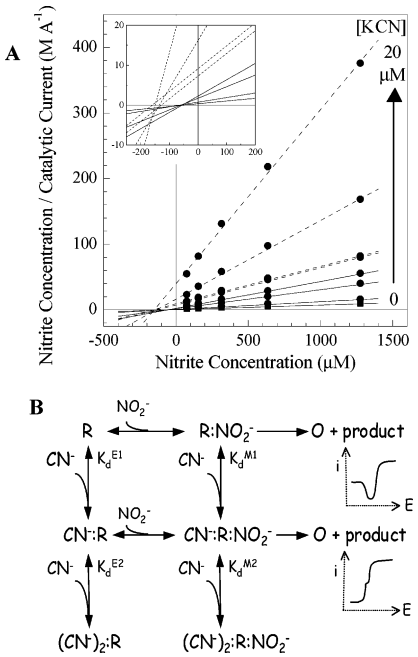

FIGURE 6: Cyanide inhibition of *E. coli* cytochrome *c* nitrite reductase. (A) Hanes plot of the nitrite reductase activity of an enzyme film poised at −403 mV in 0, 0.5, 1, 2, 4, 8, 10, and 20 μM KCN; all other conditions were as described in the legend of Figure 2A. Symbols represent experimental data and lines linear fits to the data, with broken and solid lines used for clarity. The inset shows the detail around the origin with symbols removed for clarity. (B) Schematic correlation of the mechanism of cyanide inhibition and the voltammetric response from the uninhibited enzyme and the monocyano adduct. R and O represent reduced and oxidized forms of the enzyme, respectively. See the text for details.

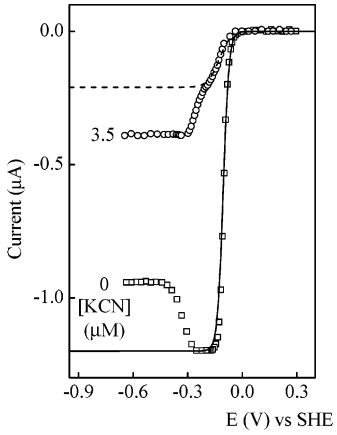

FIGURE 7: Nitrite-limited cyclic voltammetry with a film of *E. coli* cytochrome *c* nitrite reductase. Steady-state catalytic waveform of the uninhibited enzyme (□) and Nernst plot for which $n = 2$ and $E_m = -105$ mV (—). Catalytic waveform from cyanide-bound nitrite reductase (○) and Nernst plot for which $n = 1$ and $E_m = -127$ mV (- - -). Experiments were performed in 1 μM nitrite with the indicated concentration of KCN and all other conditions as described in the legend of Figure 2A. The current−potential profile of the cyanide-bound enzyme is a "reverse sweep" at 30 mV s^{-1}. See the text for details.

is centered on −248 mV, a potential positive of the reduction potentials for hemes 4 and 5 in the uninhibited enzyme (Figure 7). Since the potentials of hemes in the cyanide-complexed enzyme have not been defined, the origin of this boost is difficult to assess.

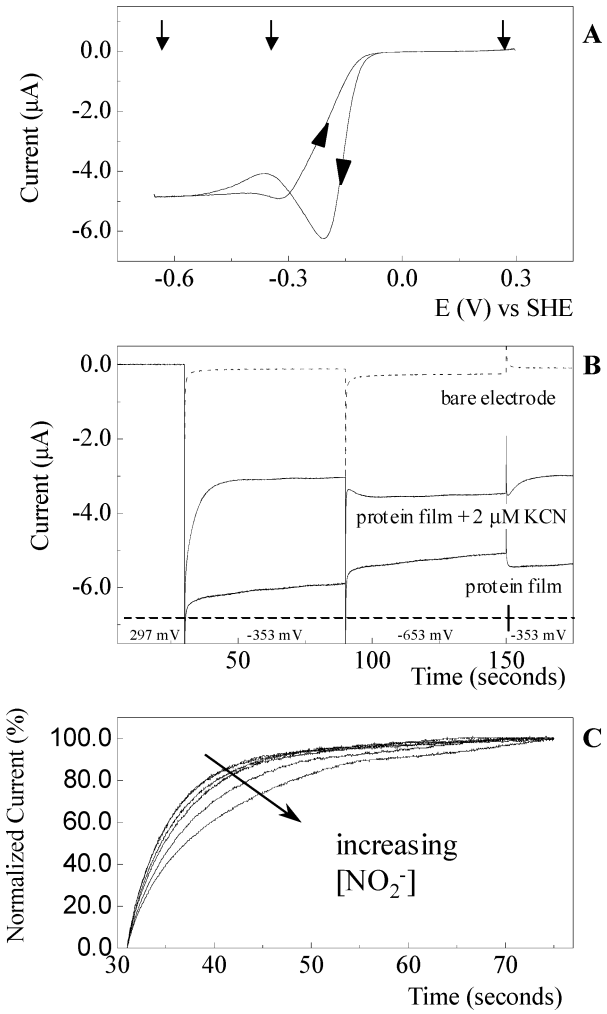

FIGURE 8: Deconvolution of time- and potential-dependent phenomena in the interaction of cyanide with films of *E. coli* cytochrome *c* nitrite reductase. (A) Typical baseline-subtracted voltammogram in 2 μM KCN and 20 μM NO_2^-, with a scan rate of 30 mV s^{-1}. The arrows indicate the potentials applied during chronoamperometry. (B) Chronoamperometry in 20 μM nitrite from a nitrite reductase film (—) with cyanide as indicated and a bare electrode (•••). (C) Normalized changes in the catalytic current from a nitrite reductase film after application of a step from 297 to −353 mV in 2 μM KCN and 5, 10, 20, 40, 80, and 160 μM nitrite. Experiments were performed with electrode rotation at 3000 rpm; other conditions were as described in the legend of Figure 2A.

Finally, we return to consider the activity−potential profiles of the forward sweeps at scan rates of ≥5 mV s^{-1} (Figures 5 and 8A). We have already seen that the peak of activity describes cyanide inhibition as the enzyme is taken from oxidized to more reduced states. Another reproducible observation is that certain combinations of scan rate and nitrite and cyanide concentration produce a window of potential in which the activity on the forward sweep is *lower* than that on the return to more positive potentials. The immediate product of cyanide association with nitrite reductase is transformed to a more active (less inhibited) form as the voltammetric sweep continues. A fuller interpretation of these aspects of voltammetry requires definition of any influence from cyanide mass transport limitations and that the effects of potential and time be resolved independently.

Limitation from cyanide mass transport can in principle be detected as a sensitivity of the catalytic waveshape to changes of electrode rotation rate. In this case, such an

analysis is complicated because the voltammetry in nitrite alone shows a marked dependence on rotation rate between 0 and 3000 rpm (*15*). However, the catalytic reduction of hydroxylamine, an alternative substrate for the enzyme ($K_M \sim 127$ mM), viewed by PFV is relatively insensitive to electrode rotation rate. At 30 mV s^{-1}, cyanide inhibition of the hydroxylamine reductase activity is slow, reversible, and triggered by reduction of the enzyme as described here for nitrite reduction (*23*). The peak of hydroxylamine reductase activity recorded on the forward sweep with an electrode rotation at 3000 rpm is reproduced at 200 rpm. Since the cyanide concentrations required to inhibit nitrite and hydroxylamine activities are comparable, the voltammetry reported here will be free from limitation by cyanide mass transport. Thus, while these experiments performed at 3000 rpm experience slight limitation from nitrite mass transport, they can be considered to provide a fare reflection of the rates of processes that would be observed at infinitely fast rotation speeds and so to reflect the relative rates of processes *intrinsic* to the enzyme film.

Resolution of the potential and time domains, intimately convoluted in cyclic voltammetry, was achieved by chronoamperometry as the potential was stepped from +297 to −353 mV and then to −653 mV before returning to −353 mV (Figure 8A). With a bare electrode placed in 20 μM nitrite, a transient current due to charging of the electrode−electrolyte interface follows each potential step (Figure 8B, dashed line). With a film of nitrite reductase in place, these transients are superimposed on much larger changes of current magnitude that report an essentially immediate change in enzyme activity in response to each change in potential. The relative current magnitudes reflect the steady-state activity of the uninhibited enzyme under these conditions (see, for example, Figure 3). The slow decrease in catalytic current magnitude is consistent with the decrease in signal magnitude noted during continuous cyclic voltammetry (*15*).

Introduction of 2 μM cyanide results in smaller catalytic currents whose relative steady-state magnitudes are consistent with those in steady-state voltammetry for these conditions (not shown but comparable to that in Figure 5A). There is a marked increase in the stability of the steady-state response as compared to that of the uninhibited enzyme and as noted in cyclic voltammetry (Figure 3). More interestingly, a slow approach to steady-state turnover follows *each* potential step as described below.

When the potential was stepped from 297 to −353 mV, the time to reach steady-state turnover reflects the *intrinsically* slow rate of cyanide association with a reduced enzyme. This rate increases as the cyanide concentration is raised but *decreases* if the nitrite concentration is increased (Figure 8C). Thus, there is *kinetic* competition between cyanide and nitrite for association with the enzyme, and it is likely that cyanide binds in the active site or one of the channels that provide access to it from the external solution (*20*, *24*).

The step from −353 to −653 mV is followed by a gradual *increase* in catalytic current that reports a gain of activity upon exposure to the lower potential (Figure 8B). Thus, transformation of the first formed cyanide adduct to a more active form is an intrinsically slow process *triggered* by exposure of the enzyme to more negative potentials. Upon returning to −353 mV, the current stabilizes to a lower level as the enzyme slowly returns to the less active form that predominates at the higher potential. The rates of these transformations appear to be independent of cyanide concentration (data not shown) so rearrangement of, or within, the cyanide-inhibited enzyme is the most likely explanation.

DISCUSSION

The interactions of cyanide and azide with cytochrome *c* nitrite reductase illustrate the complexity that can be associated with inhibitor binding to redox enzymes. PFV readily captures and deconvolves this complexity through its impact on the catalytic properties of the enzyme. In this particular case, the contrasting actions of two inhibitors have been clearly resolved and models accounting for the key voltammetric observations have been presented.

The azide-induced perturbations of *E. coli* cytochrome *c* nitrite reductase activity can be rationalized against the azide-bound structure of the homologous enzyme from *Wolinella succinogenes* (*20*). Azide is bound to residues lining the entrance to the active site, and water remains as the distal ligand to heme 1. It was suggested that binding of azide and nitrite would be mutually exclusive for steric reasons. In the case of the *E. coli* enzyme, azide and nitrite bind simultaneously when the heme 1,3 pair is reduced. That azide binds more tightly to the enzyme in the absence of nitrite is consistent with their binding in proximity to one another and most likely in positions similar to those occupied by each molecule in isolation (*17*, *20*). Certainly, retention of azide in the roof of the active site could prevent product egress from the nitrite- and azide-bound enzyme, leading to its complete inhibition. The increased affinity of azide for the enzyme upon oxidation of the heme 1,3 pair may reflect an increase in positive charge within the active site pocket.

In contrast to azide, cyanide binds more tightly to the enzyme when the heme 1,3 pair is reduced. Two other enzymes that function as nitrite reductases share this property, *Paracoccus pantotrophus* cytochrome cd_1 nitrite reductase and *E. coli* siro-heme sulfite reductase (*25*, *26*). Crystal structures of these enzymes show that cyanide binds as the distal ligand to the reduced active site heme. It is unlikely that cyanide binds in an equivalent way to cytochrome *c* nitrite reductase since it is not a competitive inhibitor of the enzyme.

Where then does cyanide bind? Given that the rate of cyanide inhibition decreases as the nitrite concentration is increased, the site of cyanide binding should be accessed through the substrate-binding pocket or the channels that lead to it from the protein surface (*20*, *24*). Cyanide could bind at the top of the substrate-binding pocket in a manner analogous to that of azide, although it is difficult to rationalize how this mechanism would lead to uncoupling of electron transfer at the heme 1,3 pair. Alternatively, cyanide could bind in the vicinity of the active site, pushing amino acid side chains into the substrate binding pocket and perhaps causing them to ligate the distal face of heme 1. There is also precedent for exogenous molecules to bind to heme proteins by displacing proteinaceous axial ligands, and cyanide could feasibly become an axial ligand to any one of hemes 1−5 through a similar process (*27*, *28*). The conformational and electronic changes that are likely to accompany these alternative modes of cyanide binding could readily

account for the uncoupling of electron transfer at the heme 1,3 pair and inactivation of the mechanism by which reduction of hemes 4 and 5 attenuates activity. A cyanide-induced conformational change could explain the slow rates of cyanide equilibration with the enzyme and the enhanced voltammetric stability of the cyanide-complexed enzyme.

It may be significant that cyanide inhibition of *Nitrosomonas europaea* hydroxylamine oxidoreductase (HAO) is also noncompetitive (*29*). HAO is an octaheme protein in which the arrangement of hemes 4−8 overlays that of hemes 1−5 in cytochrome *c* nitrite reductase despite little conservation of other structural features (*20*, *30*). Heme 4 (P460) provides the site of hydroxylamine binding and transformation and appears to be five-coordinate with histidine as an axial ligand in the absence of substrate. The unique spectroscopic properties of heme 4 allowed its identification as the cyanide-binding site, suggesting that exogenous ligands can bind to both faces of this heme. Analogy with HAO would have cyanide displacing Lys from the proximal face of heme 1 in cytochrome *c* nitrite reductase. This need not lead to complete inactivation of activity since the *E. coli* enzyme retains ca. 40% of its activity when the proximal lysine is replaced with histidine (*31*, *32*), and sequence alignments indicate that histidine is the natural ligand to heme 1 of *Campylobacter jejuni* cytochrome *c* nitrite reductase (*33*).

Whether these, or other, possibilities describe binding of cyanide to nitrite reductase, the result is two inequivalent sites for cyanide binding to, and inhibition of, the enzyme. Occupation of the higher-affinity site leads to partial noncompetitive inhibition. Occupation of the lower-affinity site leads to complete inhibition. These two cyanide-binding sites may be located within a monomer. Alternatively, they may represent binding of a single cyanide to each monomer within the dimer. In this scenario, the first cyanide would bind and completely inhibit the activity of one monomer. The properties of the second monomer would be altered such that it displays a lower affinity for cyanide and possesses catalytic properties distinct from those of the uninhibited dimer. Cyanide binding to the second monomer would then lead to the complete loss of activity from the dimer.

The challenge now is to identify the cyanide binding site(s) through spectroscopic or structural methods. The enzyme in solution assays with dithionite reduced methyl viologen as the electron donor shows patterns of cyanide, and indeed azide, inhibition similar to those defined by PFV. Thus, the protein behaves in solution as it does in the film, allowing preparation of samples for appropriate analysis. However, molecular definition of ligand binding to this multi-heme enzyme, as with many multicentered proteins, is not trivial. Absorption spectroscopy fails to distinguish adequately between the five *c*-type hemes in each monomer of nitrite reductase. EPR spectroscopy clearly resolves signals from individual ferric hemes, but the ferrous states that are of most interest in this case are invisible. Magnetic circular dichroism spectroscopy readily defines the ligation of ferric hemes but is limited in its ability to resolve the ligation of ferrous hemes (*34*). In addition, each of these spectroscopies will struggle to characterize cyanide binding to sites similar to the one occupied by azide and defined by the polypeptide rather than the hemes. These limitations of traditional spectroscopic approaches to define binding to reduced cytochrome *c* nitrite reductase serve to highlight the utility of PFV in revealing the exquisite redox-driven chemistries of redox enzymes. Experiments are now underway to define the crystal structure of reduced, cyanide-bound nitrite reductase and so provide a structural framework for further elucidation of the functional properties defined here by PFV.

CONCLUSIONS

PFV has revealed the contrasting interactions of cyanide and azide with cytochrome *c* nitrite reductase. The affinity for each molecule is critically dependent on enzyme oxidation state, although in opposing manners. The mechanisms of inhibition employed by each molecule are also distinct, but in neither case is inhibition competitive. Spectroscopic resolution of such chemistries presents a challenge in this multi-heme enzyme, but they are readily captured and resolved by PFV through simultaneous definition of enzyme activity across the electrochemical potential and time domains.

ACKNOWLEDGMENT

We are grateful to Dr. Christine Moore for purification of the protein, Dr. Hayley Angove for the first look at cyanide and nitrite reductase interactions by PFV, Prof. Jeff Cole for critical discussion, and Dr. Tom Clarke for comments on the manuscript.

SUPPORTING INFORMATION AVAILABLE

Cyclic voltammograms at 30 mV s^{-1} in solutions of 1 and 10 μM nitrite containing 0, 0.5, 1.5, and 3.5 μM cyanide and Hanes plots for cyanide and azide inhibition of nitrite reductase using dithionite-reduced methyl viologen as the electron donor. This material is available free of charge via the Internet at http://pubs.acs.org.

REFERENCES

1. Sharp, R. E., and Chapman, S. K. (1999) Mechanisms for regulating electron transfer in multi-centre redox proteins, *Biochim. Biophys. Acta 1432*, 143−158.
2. Davidson, V. L. (2002) Chemically gated electron transfer. A means of accelerating and regulating rates of biological electron transfer, *Biochemistry 41*, 14633−14636.
3. Armstrong, F. A., Heering, H. A., and Hirst, J. (1997) Reactions of complex metalloproteins studied by protein film voltammetry, *Chem. Soc. Rev. 26*, 169−179.
4. Heering, H. A., Hirst, J., and Armstrong, F. A. (1998) Interpreting the catalytic voltammetry of electroactive enzymes adsorbed on electrodes, *J. Phys. Chem. B 102*, 6889−6902.
5. Léger, C., Elliott, S. J., Hoke, K. R., Jeuken, L. J. C., Jones, A. K., and Armstrong, F. A. (2003) Enzyme electrokinetics: using protein film voltammetry to investigate redox enzymes and their mechanisms, *Biochemistry 42*, 8653−8662.
6. Armstrong, F. A. (2002) Insights from protein film voltammetry into mechanisms of complex biological electron-transfer reactions, *J. Chem. Soc., Dalton Trans.*, 661−671.
7. Elliott, S. J., Léger, C., Pershad, H. R., Hirst, J., Heffron, K., Ginet, N., Blasco, F., Rothery, R. A., Weiner, J. H., and Armstrong, F. A. (2002) Detection and interpretation of redox potential optima in the catalytic activity of enzymes, *Biochim. Biophys. Acta 1555*, 54−59.
8. Butt, J. N. (2003) Fresh perspectives on nitrogen-cycle enzymes from protein film voltammetry, *Recent Res. Dev. Biochem. 4*, 159−180.
9. Zu, Y., Shannon, R. J., and Hirst, J. (2003) Reversible, electrochemical interconversion of NADH and NAD^+ by the catalytic (I λ) subcomplex of mitochondrial NADH:ubiquinone oxidoreductase (complex I), *J. Am. Chem. Soc. 125*, 6020−6021.

10. Jones, A. K., Lamle, S. E., Pershad, H. R., Vincent, K. A., Albracht, S. P. J., and Armstrong, F. A. (2003) Enzyme electrokinetics: electrochemical studies of the anaerobic interconversions between active and inactive states of *Allochromatium vinosum* [NiFe]-hydrogenase, *J. Am. Chem. Soc. 125*, 8505−8514.
11. Anderson, L. J., Richardson, D. J., and Butt, J. N. (2001) Catalytic protein film voltammetry from a respiratory nitrate reductase provides evidence for complex electrochemical modulation of enzyme activity, *Biochemistry 40*, 11294−11307.
12. Heering, H. A., Weiner, J. H., and Armstrong, F. A. (1997) Direct detection and measurement of electron relays in a multicentered enzyme: voltammetry of electrode-surface films of *E. coli* fumarate reductase, an iron−sulfur flavoprotein, *J. Am. Chem. Soc. 119*, 11628−11638.
13. Heffron, K., Léger, C., Rothery, R. A., Weiner, J. H., and Armstrong, F. A. (2001) Determination of an optimal potential window for catalysis by *E. coli* dimethyl sulfoxide reductase and hypothesis on the role of Mo(V) in the reaction pathway, *Biochemistry 40*, 3117−3126.
14. Frangioni, B., Arnoux, P., Sabaty, M., Pignol, D., Bertrand, P., Guigliarelli, B., and Léger, C. (2004) In *Rhodobacter sphaeroides* respiratory nitrate reductase, the kinetics of substrate binding favors intramolecular electron transfer, *J. Am. Chem. Soc. 126*, 1328−1329.
15. Angove, H., Cole, J. A., Richardson, D. J., and Butt, J. N. (2002) Protein film voltammetry reveals distinctive fingerprints of nitrite and hydroxylamine reduction by a cytochrome *c* nitrite reductase, *J. Biol. Chem. 277*, 23374−23381.
16. Bamford, V., Angove, H., Seward, H., Thomson, A. J., Cole, J. A., Butt, J. N., Hemmings, A. M., and Richardson, D. J. (2002) Structure and spectroscopy of the periplasmic cytochrome *c* nitrite reductase from *Escherichia coli*, *Biochemistry 41*, 2921−2931.
17. Einsle, O., Messerschmidt, A., Huber, R., Kroneck, P. M. H., and Neese, F. (2002) Mechanism of the six-electron reduction of nitrite to ammonia by cytochrome *c* nitrite reductase, *J. Am. Chem. Soc. 124*, 11737−11745.
18. Elliott, S. J., Hoke, K. R., Heffron, K., Palak, M., Rothery, R. A., Weiner, J. H., and Armstrong, F. A. (2004) Voltammetric studies of the catalytic mechanism of the respiratory nitrate reductase from *Escherichia coli*: how nitrate reduction and inhibition depend on the oxidation state of the active site, *Biochemistry 43*, 799−807.
19. Kajie, S., and Anraku, Y. (1986) Purification of a hexaheme cytochrome *c*552 from *Escherichia coli* K12 and its properties as a nitrite reductase, *Eur. J. Biochem. 154*, 457−463.
20. Einsle, O., Stach, P., Messerschmidt, A., Simon, J., Kröger, A., Huber, R., and Kroneck, P. M. H. (2000) Cytochrome *c* nitrite reductase from *Wolinella succinogenes*. Structure at 1.6 Å resolution, inhibitor binding, and heme-packing motifs, *J. Biol. Chem. 275*, 39608−39616.
21. Vogel, A. (1961) *A Textbook of Quantitative Inorganic Analysis*, pp 271−278, Longmans, London.
22. Cornish-Bowden, A. (2001) *Fundamentals of Enzyme Kinetics*, pp 93−128, Portland Press, London.
23. Gwyer, J. D., Angove, H. C., Richardson, D. J., and Butt, J. N. (2004) Redox-triggered events in cytochrome *c* nitrite reductase, *Bioelectrochemistry 63*, 43−47.
24. Einsle, O., Messerschmidt, A., Stach, P., Bourenkov, G. P., Bartunik, H. D., Huber, R., and Kroneck, P. M. H. (1999) Structure of cytochrome *c* nitrite reductase, *Nature 400*, 476−480.
25. Jafferji, A., Allen, J. W. A., Ferguson, S. J., and Fülöp, V. (2000) X-ray crystallographic study of cyanide binding provides insights into the structure−function relationship for cytochrome cd_1 nitrite reductase from *Paracoccus pantotrophus*, *J. Biol. Chem. 275*, 25089−25094.
26. Crane, B. R., Siegel, L. M., and Getzoff, E. D. (1997) Probing the catalytic mechanism of sulfite reductase by X-ray crystallography: structures of the *Escherichia coli* hemoprotein in complex with substrates, inhibitors, intermediates, and products, *Biochemistry 36*, 12120−12137.
27. Leys, D., Backers, K., Meyer, T. E., Hagen, W. R., Cusanovich, M. A., and van Beeumen, J. J. (2000) Crystal structures of an oxygen-binding cytochrome *c* from *Rhodobacter sphaeroides*, *J. Biol. Chem. 275*, 16050−16056.
28. Lawson, D. M., Stevenson, C. E. M., Andrew, C. R., and Eady, R. R. (2000) Unprecedented proximal binding of nitric oxide to heme: implications for guanylate cyclase, *EMBO J. 19*, 5661−5671.
29. Logan, M. S. P., Balny, C., and Hooper, A. B. (1995) Reaction with cyanide of hydroxylamine oxidoreductase of *Nitrosomonas europaea*, *Biochemistry 34*, 9028−9037.
30. Igarashi, N., Moriyama, H., Fujiwara, T., Fukumori, Y., and Tanaka, N. (1997) The 2.8 Å structure of hydroxylamine oxidoreductase from a nitrifying chemoautotrophic bacterium, *Nitrosomonas europaea*, *Nat. Struct. Biol. 4*, 276−284.
31. Eaves, D. J., Grove, J., Staudenmann, W., James, P., Poole, R. K., White, S. A., Griffiths, I., and Cole, J. A. (1998) Involvement of products of the nrfEFG genes in the covalent attachment of haem *c* to a novel cysteine-lysine motif in the cytochrome *c*552 nitrite reductase from *Escherichia coli*, *Mol. Microbiol. 28*, 205−216.
32. Pisa, R., Stein, T., Eichler, R., Gross, R., and Simon, J. (2002) The nrfI gene is essential for the attachment of the active site haem group of *Wolinella succinogenes* cytochrome *c* nitrite reductase, *Mol. Microbiol. 43*, 763−770.
33. Simon, J. (2002) Enzymology and bioenergetics of respiratory nitrite ammonification, *FEMS Microbiol. Rev. 26*, 285−309.
34. Gadsby, P. M. A., and Thomson, A. J. (1990) Assignment of the axial ligands of ferric-ion in low-spin hemoproteins by near-infrared magnetic circular dichroism and electron paramagnetic resonance spectroscopy, *J. Am. Chem. Soc. 112*, 5003−5011.

BI049085X